



HAL
open science

Knockdown of calpain1 in lumbar motoneurons reduces spasticity after spinal cord injury in adult rats

Marjorie Kerzonkuf, Jérémy Verneuil, Cécile Brocard, Nejada Dingu, Virginie Trouplin, Jose Jorge Ramirez Franco, Marc Bartoli, Frédéric Brocard, Hélène Bras

► To cite this version:

Marjorie Kerzonkuf, Jérémy Verneuil, Cécile Brocard, Nejada Dingu, Virginie Trouplin, et al.. Knockdown of calpain1 in lumbar motoneurons reduces spasticity after spinal cord injury in adult rats. *Molecular Therapy*, 2024, 10.1016/j.ymthe.2024.01.029 . hal-04483886

HAL Id: hal-04483886

<https://amu.hal.science/hal-04483886v1>

Submitted on 29 Feb 2024

HAL is a multi-disciplinary open access archive for the deposit and dissemination of scientific research documents, whether they are published or not. The documents may come from teaching and research institutions in France or abroad, or from public or private research centers.

L'archive ouverte pluridisciplinaire **HAL**, est destinée au dépôt et à la diffusion de documents scientifiques de niveau recherche, publiés ou non, émanant des établissements d'enseignement et de recherche français ou étrangers, des laboratoires publics ou privés.



Distributed under a Creative Commons Attribution - NonCommercial - NoDerivatives 4.0 International License

Knockdown of calpain1 in lumbar motoneurons reduces spasticity after spinal cord injury in adult rats

Marjorie Kerzonkuf,^{1,3} Jérémy Verneuil,^{1,3} Cécile Brocard,^{1,3} Nejada Dingu,¹ Virginie Trouplin,¹ Jose Jorge Ramirez Franco,¹ Marc Bartoli,² Frédéric Brocard,^{1,4} and Hélène Bras^{1,4}

¹Institut des Neurosciences de la Timone (UMR7289), Aix-Marseille Université and CNRS, Marseille, France; ²Institut Marseille Maladies Rares (MarMaRa), Aix-Marseille Université and INSERM, Marseille, France

Spasticity, affecting ~75% of patients with spinal cord injury (SCI), leads to hyperreflexia, muscle spasms, and cocontractions of antagonist muscles, greatly affecting their quality of life. Spasticity primarily stems from the hyperexcitability of motoneurons below the lesion, driven by an upregulation of the persistent sodium current and a downregulation of chloride extrusion. This imbalance results from the post-SCI activation of calpain1, which cleaves Nav1.6 channels and KCC2 cotransporters. Our study was focused on mitigating spasticity by specifically targeting calpain1 in spinal motoneurons. We successfully transduced lumbar motoneurons in adult rats with SCI using intrathecal administration of adeno-associated virus vector serotype 6, carrying a shRNA sequence against calpain1. This approach significantly reduced calpain1 expression in transduced motoneurons, leading to a noticeable decrease in spasticity symptoms, including hyperreflexia, muscle spasms, and cocontractions in hindlimb muscles, which are particularly evident in the second month post-SCI. In addition, this decrease, which prevented the escalation of spasticity to a severe grade, paralleled the restoration of KCC2 levels in transduced motoneurons, suggesting a reduced proteolytic activity of calpain1. These findings demonstrate that inhibiting calpain1 in motoneurons is a promising strategy for alleviating spasticity in SCI patients.

INTRODUCTION

Spinal cord injuries (SCIs) represent a major global health issue, with ~900,000 new cases each year. A predominant complication in 75% of SCI patients is spasticity, a sensorimotor disorder characterized by exaggerated tendon reflexes (hyperreflexia), spontaneous muscle contractions (spasms), cocontractions of antagonist muscles, and clonus leading to reduced mobility, pain, and disrupted sleep. This condition significantly impedes the rehabilitation process and profoundly diminishes the quality of life.¹ Baclofen (Lioresal, a GABA_B agonist), the main drug currently used to treat spasticity, presents important side effects such as increased muscle weakness, fatigue, dizziness, and drowsiness.² Meanwhile, intramuscular injections of botulinum toxin A (peripheral denervation) offer only temporary relief for focal spasticity.³ A more effective therapeutic approach will stem from an in-depth exploration

of the pathophysiological mechanisms behind spasticity, with the goal of targeting the causes rather than simply alleviating symptoms.

The pathophysiology of spasticity involves motoneuron hyperexcitability,^{2,4-6} which is associated with increased persistent sodium and calcium currents, along with synaptic disinhibition.⁷⁻¹³ This latter aspect is due to changes in glycine receptors and a reduction in the chloride extruder KCC2,¹³⁻¹⁹ which exacerbates spasticity in both humans and rodents. Such an excitatory/inhibitory imbalance leads to self-sustained spiking activity in sublesional motoneurons, causing prolonged muscle contractions that can be either evoked or spontaneous.²⁰⁻²⁴ Calpain, a protease activated under conditions of excitotoxicity and increased intracellular calcium, plays a crucial role in this process. It upregulates persistent sodium currents and disrupts chloride homeostasis by cleaving Nav1.6 channels and the chloride extruder KCC2, respectively.^{13,16} Identifying calpains as key contributors to motoneuron hyperexcitability post-SCI positions them as primary targets for spasticity treatment, offering a new direction for therapeutic intervention.

Of the 16 identified mammalian calpains, calpain1 and calpain2 are ubiquitous and show different Ca²⁺ sensitivity (in the range of μ M for calpain1 and mM for calpain2).²⁵ Shortly after SCI, there is a marked increase in calpain expression at the injury site,²⁶⁻²⁸ especially in motoneurons.²⁹ Notably, calpain1 but not calpain2 is associated with the tissue damage following SCI.^{26,29,30} In the chronic phase, gene expression analysis in motoneurons below the SCI site shows an increase in calpain1 expression.³¹ These changes underscore the dynamic regulation of calpain activity after SCI. The present study investigates the role of

Received 20 April 2023; accepted 23 January 2024;
<https://doi.org/10.1016/j.ymthe.2024.01.029>.

³These authors contributed equally

⁴These authors contributed equally

Correspondence: Frédéric Brocard, Institut des Neurosciences de la Timone (UMR7289), Aix-Marseille Université and CNRS, Marseille, France.

E-mail: frederic.brocard@univ-amu.fr

Correspondence: Hélène Bras, Institut des Neurosciences de la Timone (UMR7289), Aix-Marseille Université and CNRS, Marseille, France.

E-mail: helene.bras@univ-amu.fr

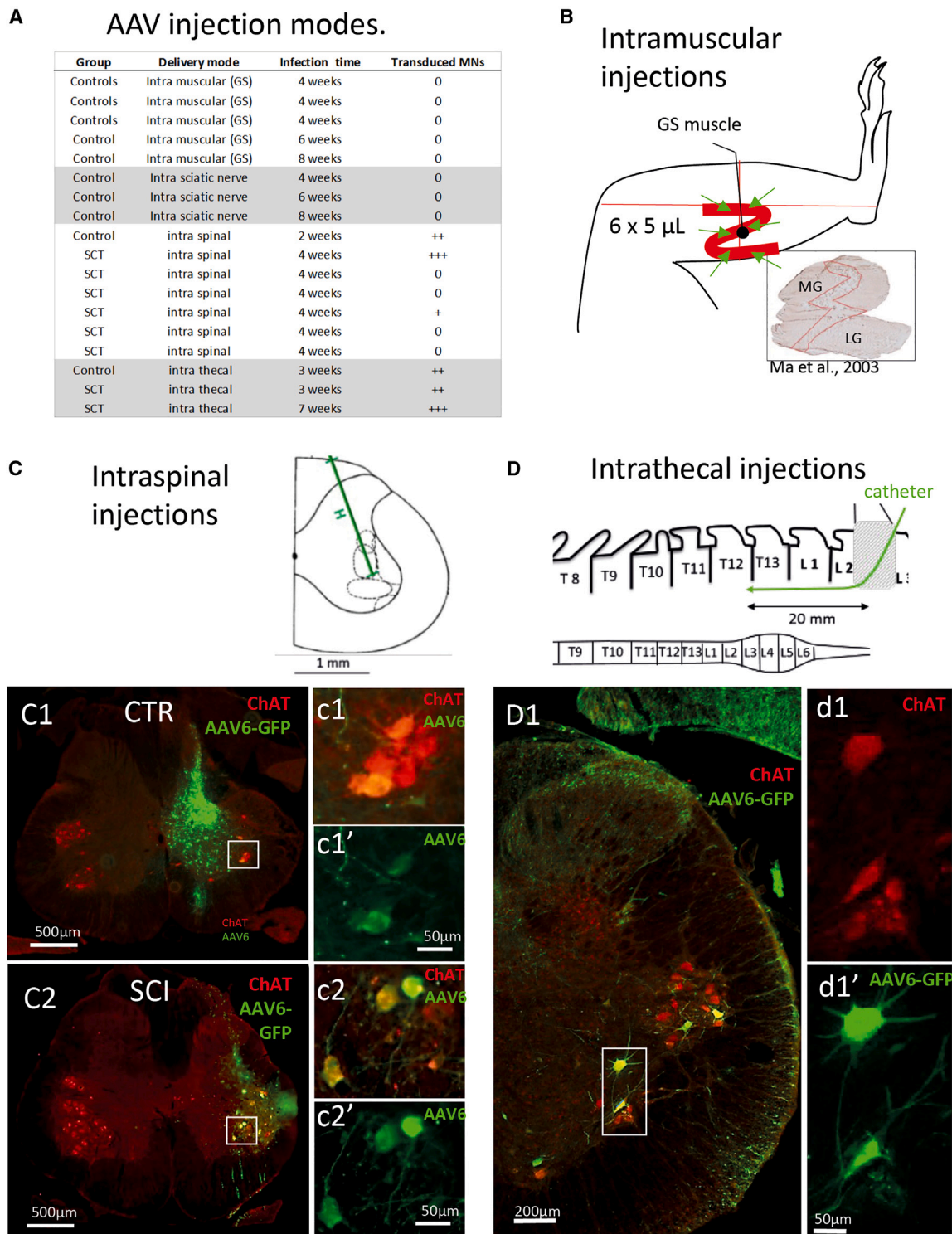


Figure 1. AAV6 injection modes

(A) Summary table outlines the results from various AAV6 administration methods in both control/intact or transected (SCT) rats across different infection times. The density of transduced motoneurons was qualitatively assessed as nonexistent (0), very sparse (+), fair (++), or abundant (+++). (B) The i.m. injections targeted the medial GS muscle at multiple sites (indicated by green arrows), focusing on motor endplates along the muscle (illustrated by the red line).³⁴ (C) The i.s. injections (top, experimental design) resulted

(legend continued on next page)

calpain1 in SCI-induced spasticity in adult rats. Using adeno-associated viral vector serotype 6 (AAV6), we targeted calpain1 in sublesional motoneurons. The treatment led to a substantial decrease in postinjury hyperreflexia, muscle spasms, and cocontractions, along with the normalization of KCC2 membrane levels. In addition to enhancing our understanding of the pathophysiology of spasticity, these findings open up new therapeutic avenues that directly target the molecular mechanisms underlying spastic symptoms.

RESULTS

Optimizing AAV6 delivery to lumbar spinal motoneurons in adult rats

To identify the optimal method for delivering AAV6 to lumbar spinal motoneurons in adult rats, we conducted a series of preliminary experiments with 18 animals (Figure 1A). Our initial attempt involved intramuscular (i.m.) injection of AAV6-GFP-short hairpin RNA (shRNA)-CAPN1 into the gastrocnemius (GS) muscle of 5 rats (Figure 1B). Unfortunately, this method did not result in any transduced GFP⁺ motoneurons in the lumbar spinal cord, regardless of the time elapsed postinjection (4, 6, and 8 weeks). A similar lack of transduction efficiency was observed when AAV6-GFP-shRNA-CAPN1 was injected into the sciatic nerve of 3 rats (Figure 1A). We then explored the intraspinal injection as an alternative. This approach successfully resulted in transduced GFP⁺ motoneurons (Figures 1C1 and 1C2), but only in 3 out of 7 animals (Figure 1A). Notably, we also observed GFP⁺ interneurons along the path of the cannula in the dorsal and intermediate medulla (Figures 1C1 and 1C2), which raised concerns about unintentionally affecting interneurons within the premotor network. Our final approach involved intrathecal (i.t.) delivery of AAV6 (Figure 1D). Three weeks after injection, we noted a moderate density in transduced motoneurons in 1 control and 1 SCI animal (Figures 1A and 1D1). Extending the infection period to 7 weeks significantly increased the density of transduced lumbar motoneurons. More important, the majority of the infected neurons were identified as motoneurons (GFP⁺, choline acetyltransferase-positive [ChAT⁺]), with only a few transduced interneurons (GFP⁺, ChAT⁻). These results indicate that i.t. administration is the most efficient method for targeting spinal motoneurons in adult rats. Therefore, we selected this route for all of our subsequent experiments.

Evaluating shRNA-CAPN1 efficacy to reduce CAPN1 expression

The efficacy of AAV6-shRNA-CAPN1 treatment to reduce CAPN1 was first evaluated *in vitro* by analyzing calpain1 levels by western blotting. HEK293 cells were transfected with calpain1-encoding plasmid alone (Figure 2A1, left), or cotransfected with calpain1 + shRNA luciferase used as a control (Figure 2A1, center), or with calpain1 + shRNA calpain1 (Figure 2A1, right). The calpain1 expression was significantly reduced by 85% compared to the control group

(Figure 2A2; $p < 0.001$; Mann-Whitney test). This substantial decrease highlights the effectiveness of shRNA-calpain1 in targeting and reducing calpain1 expression at the cellular level.

We then extended our investigation to an *in situ* analysis, focusing on the impact of the shRNA-CAPN1 on calpain1 expression in sublesional motoneurons. We performed quantitative calpain1 immunofluorescence assessments on confocal sections showing pairs of motoneurons (Figures 2B and 2C). Each pair consisted of 1 GFP⁺ (transduced) and one GFP⁻ (nontransduced) motoneuron from 2 groups of SCI rats, treated with either shRNA-CAPN1 or shRNA-scramble (Figures 2B1 and 2C1). The motoneuron transduced with shRNA-CAPN1 showed a significant 42% decrease in cytoplasmic calpain1 levels compared to nontransduced motoneurons (Figures 2B2 and 2D1; $p < 0.001$; Mann-Whitney test). In contrast, motoneurons transduced with shRNA-scramble exhibited calpain1 levels similar to those in nontransduced motoneurons (Figures 1C2 and 2D2; $p > 0.05$, Mann-Whitney test). These findings validate the precise targeting and knockdown efficacy of shRNA-CAPN1 in reducing calpain1 expression in lumbar motoneurons.

Therapeutic impact of motoneuronal knockdown of calpain1 on spasticity

To assess the impact of shRNA-mediated reduction of calpain1 in motoneurons on spasticity after SCI, we performed electromyography (EMG) measurements on the GS and tibialis anterior (TA) muscles. This was initiated 4 weeks following the i.t. administration of AAV6. Our analysis focused on the evolution and characteristics of muscle spasms, including their frequency, duration, amplitude, and the number of cocontractions, key indicators of spasticity.

In the scramble group, a notable and progressive increase in cumulative GS and TA muscle spasms was observed, culminating at 7 weeks post-SCI (Figures 3A, 3B, and 3E; $p < 0.001$; 2-way ANOVA). Linear regression analysis confirmed a significant deviation of the slope from zero ($p < 0.001$), indicative of escalating spastic activity. This pattern was also evident when considering the GS and TA muscles individually (Figures 3F and 3G; $p < 0.001$; 2-way ANOVA), with an associated increase in GS/TA cocontractions (Figure 3H; $p < 0.05$; 2-way ANOVA). In contrast, the shRNA group displayed stable spasm counts throughout the study period (Figures 3C–3G; $p > 0.05$; 2-way ANOVA), with the linear regression slope showing no significant deviation from zero ($p > 0.05$). Remarkably, the shRNA group exhibited significantly fewer spasms than the scramble group (Figure 3E; $p < 0.01$; 2-way ANOVA), particularly in the GS muscle from week 6 post-SCI (Figure 3F; $p < 0.05$; 2-way ANOVA). The TA muscle exhibited a trend toward spasm reduction, although this did not achieve statistical significance in the 7-week period (Figure 3G;

in transfection (GFP, green) of ChAT⁺ motoneurons (red) in both control (C1, CTR) and transected (C2, SCT) animals. Many interneurons on the path of the cannula were also GFP⁺ in the dorsal and intermediate laminae. The insets are magnifications of the selected area. Scale bar, 500 μ m in main image and 50 μ m in insets. (D) Schematic representation of an i.t. injection (top) shows the process following laminectomy at the L2–L3 vertebrae. A cannula was inserted forward by 2 mm to reach the rostral lumbar spinal segments (L2). (D1) ChAT⁺ motoneurons (red) were transduced (green, GFP), with only a few interneurons showing GFP⁺. The insets are magnifications of the selected area. Scale bar, 200 μ m in main image and 50 μ m in insets.

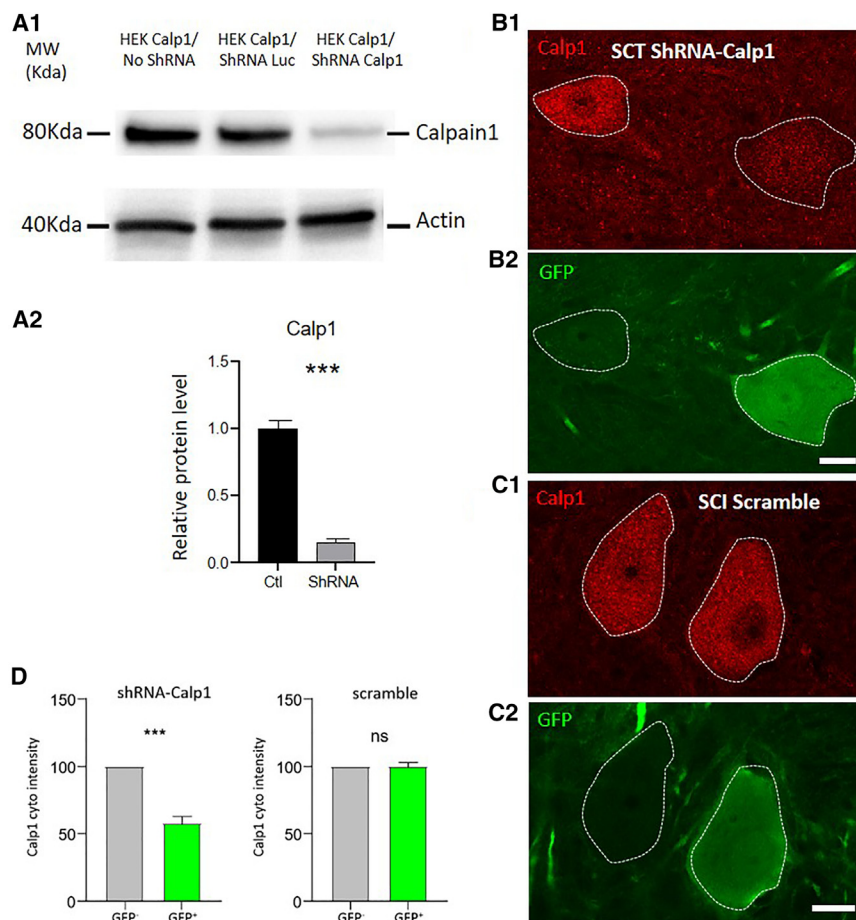


Figure 2. Decrease in cytoplasmic expression of calpain1 in shRNA-CAPN1-transduced lumbar motoneurons of SCI rats

(A1) Calpain1 immunoblots of the total fraction of HEK293 cells transfected either with calpain1 (left) or calpain1 + shRNA luciferase as a control (center) or calpain1 + shRNA calpain1 (right). The 80-kDa bands correspond to the full-length calpain1 native protein, whereas the 40-kDa bands correspond to actin, serving as an internal control. (A2) Quantitative analysis of calpain1 expression in HEK293 cells transfected only with calpain1 and calpain1/luciferase ($n = 8$ CTR/6 shRNA). (B1-2 and C1-2) Confocal microscopy sections of pairs of motoneurons, each pair consisting of a transfected (green) and a nontransfected cell, either with AAV6-GFP-shRNA-CAPN1 (B1) or AAV6-GFP-shRNA-scramble (C1), and immunostained for calpain1 (B2, C2, red). Scale bar, 20 μm . (D1 and D2) Histograms comparing the relative intensity of cytoplasmic calpain1 in nontransfected (gray) versus transfected (green) motoneurons, with data from shRNA-CAPN1 (D1, $n = 23$ pairs) and shRNA-scramble (D2, $n = 22$ pairs) treatments. n.s., nonsignificant; *** $p < 0.05$ (Mann-Whitney test for A2, D1, and D2). Data are expressed as mean \pm SEM in A2, and mean \pm SD in D1, D2).

Distribution of transduced cells in the sublesional spinal cord

To evaluate the degree of motoneuron transduction, we analyzed the sublesional spinal cord at the conclusion of the EMG recording period. Our examination revealed effective transduction (ChAT⁺/GFP⁺) of motoneurons in the ventrolateral region of the lumbar spinal cord

in all animals, regardless of whether they received AAV6-GFP-shRNA-CAPN1 or the scramble treatment, with only minimal interneuron infection observed (Figure 5A). Significantly, there was no transduction noted in the dorsal root ganglia (Figure 5B). A detailed examination of histological rostro-caudal sections showed bilateral transduction of motoneurons across the lumbar segments, with a majority of the transduced motoneurons being located between segments L3 and L5 (Figure 5C). These segments, known to contain the motoneuron pools for the GS and TA muscles, demonstrated the targeted efficacy of our approach. The transfection rates were similar for both GS motoneurons (40.8%, 31 of 76) and TA motoneurons (38%, 35 of 92), confirming effective targeting of the motoneuron pools for both muscle groups. Further validation of our findings came from clearing the entire lumbar spinal cord, revealing that up to 70% of ChAT⁺ neurons at the L4–L5 lumbar segment colocalized with GFP, indicating a high success rate of transduction (Figures 5D–5G).

Upregulation of the membrane levels of KCC2 in SCI motoneurons transduced with shRNA-CAPN1

Following SCI, the reduction of KCC2 in sublesional motoneurons due to calpain activity weakens postsynaptic inhibition and contributes to

$p > 0.05$; 2-way ANOVA). More important, calpain1 knockdown led to a significant decrease in GS/TA cocontractions (Figure 3H; $p < 0.05$; 2-way ANOVA). Furthermore, the duration and amplitude of GS and TA muscle spasms remained unchanged post-SCI and did not significantly differ between the groups (Figures 3I–3L).

We also monitored responses to tail pinch, with sample traces for both groups at various time points illustrated in Figures 4A–4D. In the scramble group, evoked muscle activity in the GS and TA increased as early as 5 and 7 weeks post-SCI, respectively, consistent with typical spasticity development (Figures 4E and 4F, black traces, 2-way ANOVA). However, rats treated with AAV6-GFP-shRNA-CAPN1 maintained stable muscle responses to sensory stimulation, with notably reduced evoked GS activity from week 6 onward compared to scramble animals (Figure 4E; $p < 0.001$; 2-way ANOVA) and decreased TA muscle hyperactivation by week 7 (Figure 4F; $p < 0.01$; 2-way ANOVA).

In summary, our gene therapy approach, focusing on the downregulation of calpain1 in lumbar motoneurons post-SCI, effectively reduced muscle spasms, cocontractions, and hyperreflexia, thereby preventing the development of severe spasticity.

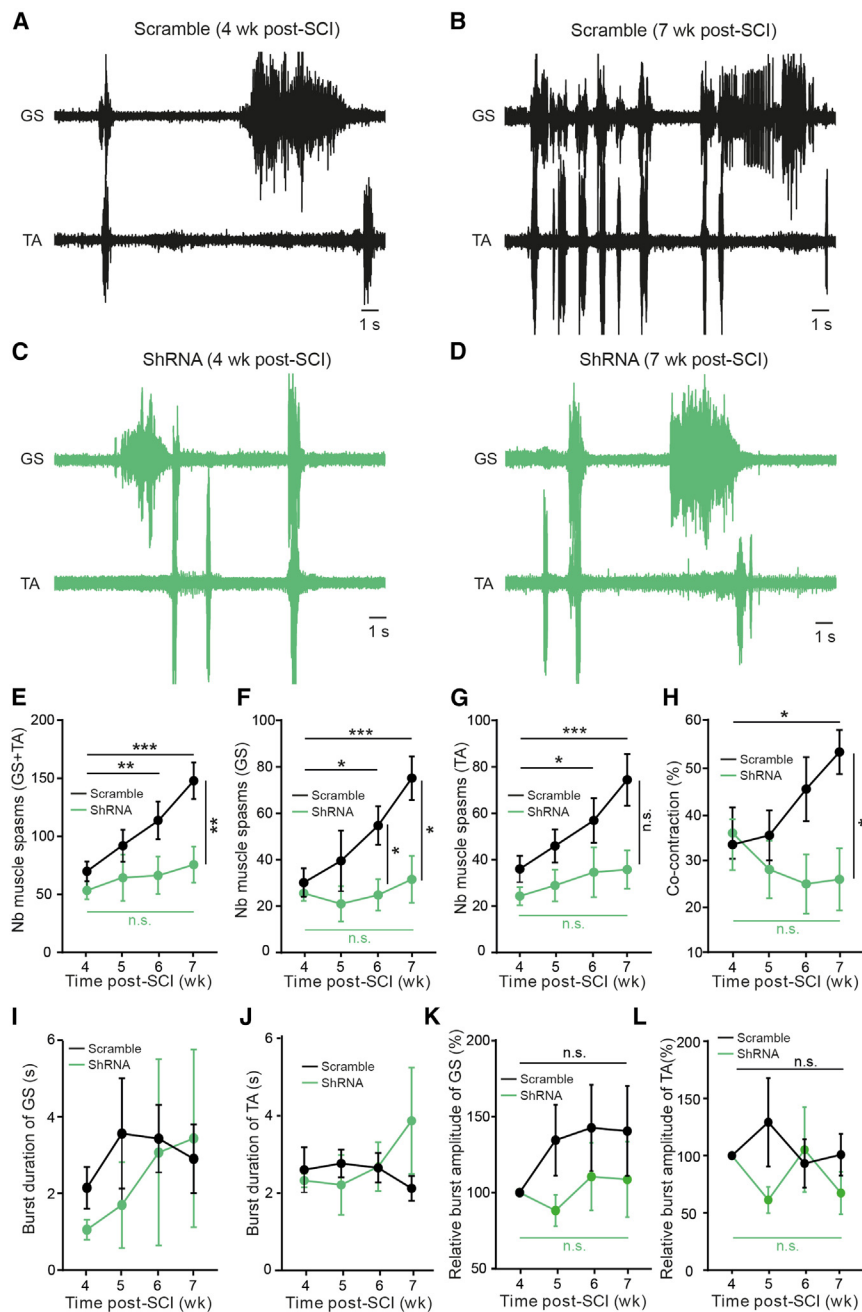


Figure 3. Reduced spontaneous muscular activities in SCI rats injected with shRNA-CAPN1

(A–D) Representative EMG recordings of involuntary muscular contractions in the GS and TA muscles from adult rats with SCI. The recordings compare 2 groups: rats transduced with a scrambled sequence (A and B, black traces, $n = 8$ rats) and those treated with shRNA targeting calpain1 (C and D, green traces, $n = 7$ rats) at 2 time points, 4 weeks (A and C) and 7 weeks (B and D) after SCI. (E–G) Comparative analysis of muscle spasms recorded in the GS and TA muscles over a period of 4–7 weeks post-SCI. Data include the total number of spasms across both muscle groups (E), as well as detailed counts for each muscle individually, GS (F) and TA (G). (H) Rates of cocontractions between the GS and TA muscles. (I–L) Spasm duration and relative amplitude for both muscles (I and K for GS and J and L for TA). Data are expressed as mean \pm SEM, with burst amplitudes normalized to values at week 4. * $p < 0.05$; ** $p < 0.01$; *** $p < 0.001$ (2-way ANOVA and Holm-Sidak’s post hoc test for E–L).

compared to nontransduced motoneurons (Figure 6B1, left; $p < 0.001$; t test). In contrast, motoneurons transduced with shRNA-scramble showed no significant difference in KCC2 levels (Figure 6B1, right; $p > 0.05$; t test). In addition, we found no significant difference in the diameter of motoneurons (Figure 6B2; $p > 0.05$; t test) or in intracytoplasmic ChAT levels (Figure 6B3; $p > 0.05$; t test). This consistency across all of the groups rules out any potential bias due to motoneuron size or neurotransmitter synthesis, confirming cellular health.

Altogether, these findings demonstrate that the i.t. injection of AAV6-shRNA-CAPN1 effectively prevents the pathological decrease in KCC2 in sublesional transduced motoneurons, underscoring its potential as a post-SCI therapeutic strategy.

DISCUSSION

Our preclinical study represents a major leap in gene therapy, aimed at alleviating spasticity after SCI by targeting spinal motoneurons. By using i.t. administration of AAV6-GFP-shRNA-CAPN1, we specifically targeted calpain1 in lumbar motoneurons of adult SCT rats. This precise approach led to a substantial reduction in hindlimb muscle spasticity, evidenced by a notable decrease in muscle spasms alongside diminished hyperreflexia and fewer muscle cocontractions. In parallel to these functional improvements, we observed a decrease in the cytoplasmic expression of calpain1 and an increase in KCC2 expression within the targeted motoneurons. This dual molecular change highlights the effectiveness of our gene therapy strategy in addressing

spasticity.¹³ To understand the impact of calpain1 knockdown on KCC2 expression, we quantified KCC2 immunofluorescence in these motoneurons. Similar to our approach for calpain1 immunofluorescence quantification, we analyzed pairs of motoneurons on the same confocal section (Figures 6A1 and 6A2). Each pair consisted of 1 transduced (ChAT⁺/GFP⁺) and 1 nontransduced (ChAT⁺/GFP⁻) motoneuron from SCI rats treated with either shRNA-CAPN1 or shRNA-scramble. Our findings revealed a significant 16% increase in membrane KCC2 levels in shRNA-CAPN1 transduced motoneurons

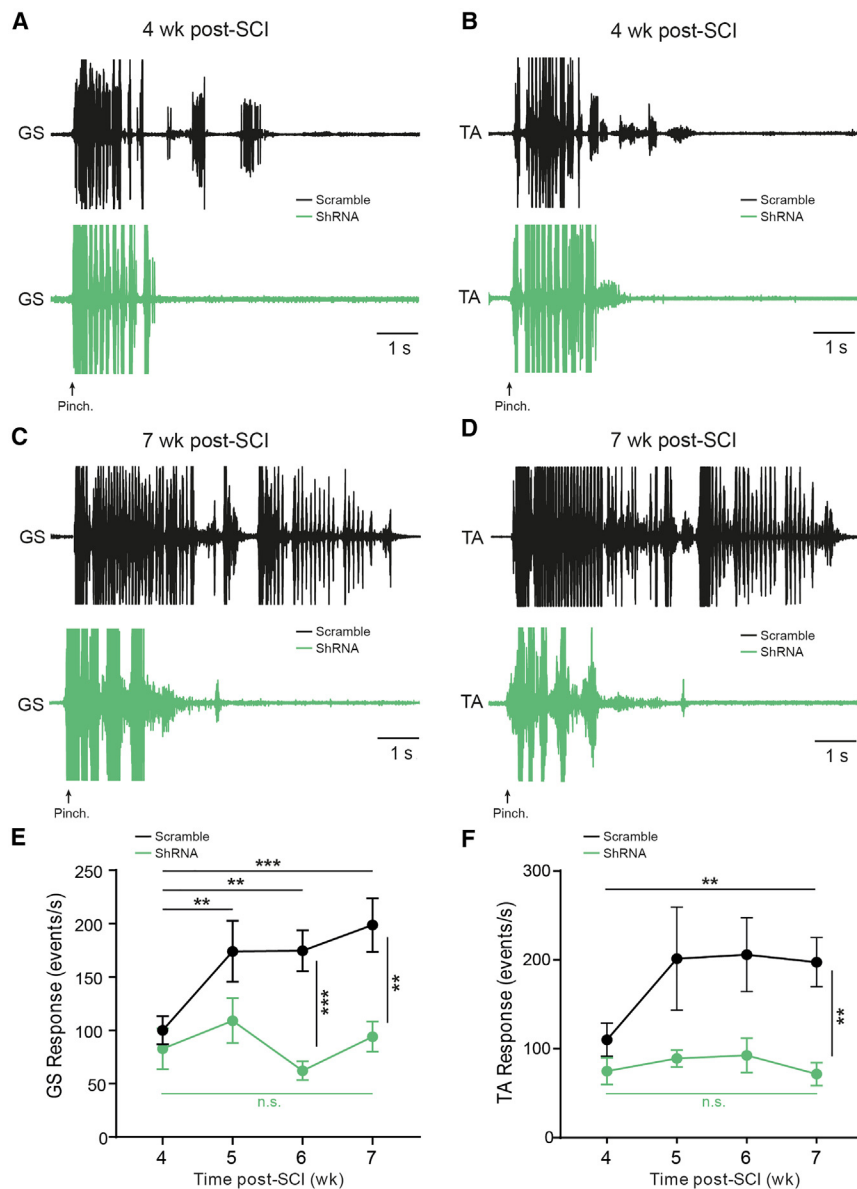


Figure 4. Decrease in hyperreflexia in SCI rats injected with shRNA-CAPN1

(A–D) Representative EMG responses in the GS; (A and C) and TA (B and D) muscles evoked by tail stimulation (arrow) at 4 weeks (A and B) and 7 weeks (C and D) after SCI in rats treated either with the scramble (black, $n = 8$ rats) or shRNA-CAPN1 (green, $n = 7$ rats). (E and F) Mean number of events per second detected in the evoked EMG response recorded from GS (E) or TA (F) muscles over a period of 4 to 7 weeks post-SCI in rats treated either with the scramble (black) or shRNA-CAPN1 (green). Data are normalized to values at week 4 and expressed as mean \pm SEM. * $p < 0.05$; ** $p < 0.01$; *** $p < 0.001$ (2-way ANOVA and Holm-Sidak's post hoc test for E and F).

the delivery of vectors to motoneurons. Success in selective motoneurons transduction has been documented in several studies, notably with AAV2 in adult mice and AAV6 in neonatal mice.^{34,35} Despite these successes, challenges remain. The i.m. and i.n. routes often led to unintentional transfection of sensory neurons (evidenced with AAV8 and AAV9 in neonatal mice)³⁶ and unexpected motoneurons after single muscle injection (AAV9, adult mice).³⁷ In addition, instances of weak or failed transfection have been reported (AAV2, -3, -4, -5, -6, and -9),^{38–40} including in our own findings with AAV6 (Figure 1). These negative results may be due to factors such as insufficient viral particle concentration, the developmental stage of the animal, or inadequate retrograde transport time. The i.v. administration led to the transfection of not only motoneurons but also interneurons, glial cells, and dorsal root ganglia (DRG) sensory neurons.^{36,41–43} The i.s. injection, in contrast, results in the transfection of only a small number of motoneurons.⁴⁴ This is due to the limited spread of the virus, potentially affecting only 3% of the lumbar spinal cord, a scope likely too narrow to significantly affect spasticity readout.

the complex pathology of SCI-induced spasticity. Beyond demonstrating the potential of gene therapy in neuromuscular rehabilitation post-SCI, our study lays the groundwork for further therapeutic developments in this domain.

AAV route of administration to efficiently target lumbar motoneurons in adult rats

Several preclinical studies have aimed to administer AAV-mediated gene therapy to spinal motoneurons to treat motoneuron disorders.^{32,33} Among the 5 routes of administration examined, namely i.m., intranerve (i.n.), intravenous (i.v.), intraspinal (i.s.) and i.t., i.m. and i.n. have been highlighted as being the most effective³² because they leverage the axonal retrograde transport machinery, facilitating

Moreover, the transduction is not confined to motoneurons alone but also extends to interneurons, posing a risk of disrupting premotor network functions (see Figure 1C). In contrast, our study shows that the i.t. administration of AAV6 stands out for its efficacy and reproducibility, achieving motoneuron transduction with minimal impact on interneurons and DRG sensory neurons. This specific transfection pattern may be related to the predominant retrograde transport properties of AAV6.⁴⁵ After i.t. administration, AAV6 likely disseminates through the cerebrospinal fluid, interacting with ventral roots, possibly at nonmyelinated segments such as the nodes of Ranvier. The virus then travels retrogradely to motoneuron somas. This naturally leads to a higher transfection efficiency in motoneurons as opposed to DRG and interneurons, which are less accessible via this route. Our

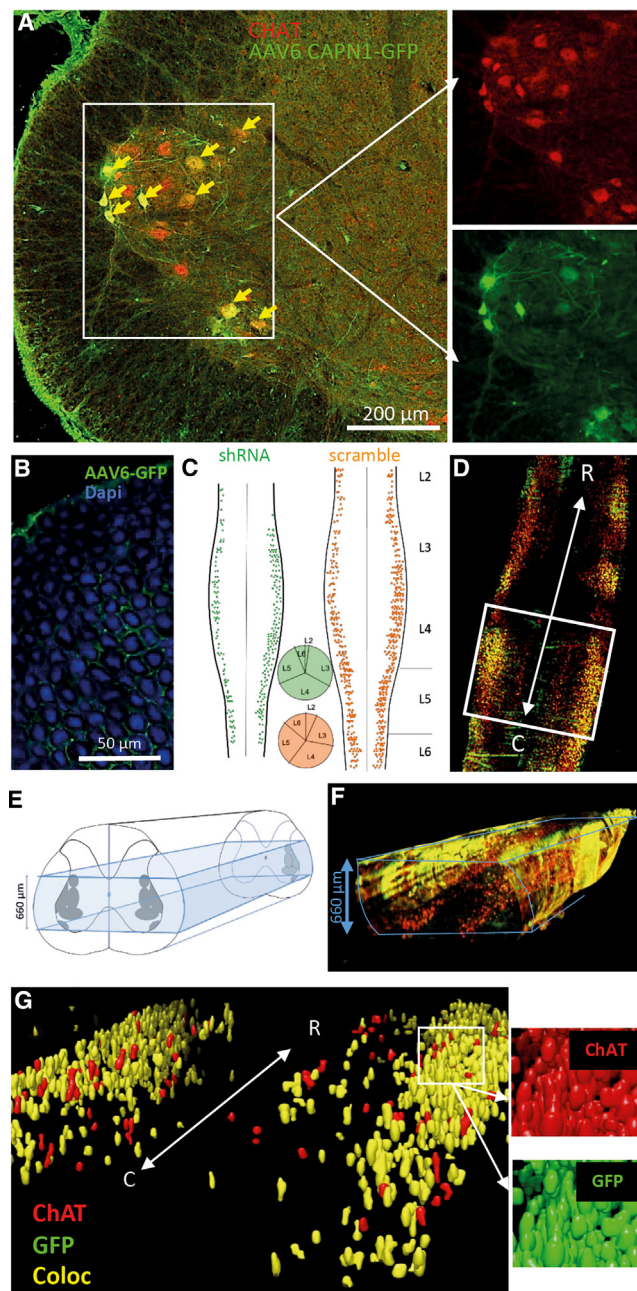


Figure 5. Distribution of transduced motoneurons following i.t. administration of AAV6 carrying shRNA-CAPN1 or shRNA-scramble in SCI adult rats

(A) Confocal microscopy transverse section from the L4 lumbar segment ($\times 10$ magnification), 7 weeks after i.t. delivery of AAV6-GFP-shRNA-CAPN1, displays extensive transduction (GFP⁺, green) in presumptive motoneurons (ChAT⁺, red). Scale bar, 200 μ m. Insets are magnifications of the selected area. (B) Confocal image showing the absence of transduction in the DRG following i.t. injection of AAV6-GFP-shRNA-CAPN1. Scale bar, 50 μ m. (C) Mapping of the rostro-caudal distribution of transduced motoneurons along L2–L6 lumbar spinal segments, based on ChAT immunostaining in SCI rats after i.t. injection of shRNA-CAPN1 (n = 3 spinal cords, left) or shRNA-scramble (n = 3 spinal cords, right). Each dot

findings are consistent with evidence indicating that AAV6 excels in motoneuron transduction after i.t. injection in adult mice.⁴⁴ We conclude that AAV6, when i.t. administered, offers a specific and effective method for transducing spinal motoneurons in adult rats, presenting a promising avenue for gene therapy in motoneuron disorders.

Time course of spasticity

Initially, spinal shock typically results in reduced muscle tone, which subsequently transitions into increased tone over time.⁴⁶ However, the temporal progression of spasticity following SCI is a multifaceted process, influenced by several physiological and pathological factors. This complexity is evident in rat models, where the manifestation of spasticity varies according to the nature and site of the injury. For example, a T8 hemisection often results in maximum muscle tone at ~ 3 weeks postinjury, with this heightened tone persisting at $\sim 75\%$ of its peak for up to 8 weeks.⁴⁷ However, midthoracic contusion injuries are characterized by an early increase in transient tonic spasticity ~ 2 weeks postinjury, which temporarily diminishes and then reappears permanently after 1 month.⁴⁸ Moreover, in the scenario of complete sacral SCI in rats, spasticity significantly increases starting from 2 weeks postinjury, continues to escalate for approximately 2 months, and thereafter remains at a heightened level.⁴⁹ The diverse timing and progression of spasticity underscore the importance of considering the specific parameters of injury in SCI research and treatment development. Our study adds to this understanding by providing a detailed time line of spastic symptoms, as we monitored spontaneous and evoked EMG activities in the GS and TA antagonistic muscles of the ankle joint. Following complete spinal cord transection at the thoracic level, we observed a pronounced increase in hyperreflexia in response to sensory stimuli between the fourth and fifth week post-SCI in these muscles. Interestingly, although hyperreflexia stabilized, muscle spasms continued to increase. This divergence in the trajectories of hyperreflexia and muscle spasms post-SCI suggests that although they share some underlying pathophysiological mechanisms, they also exhibit alterations specific to each condition. Muscle spasms may denote more enduring and complex changes at the central level, whereas hyperreflexia could additionally signify maladaptive plasticity within reflex pathways, potentially including alterations such as the sprouting of primary afferent fibers following SCI.⁵⁰ Altogether, our finding of spasticity persisting until week 7 post-SCI aligns with existing literature showing a gradual increase in spinal excitability post-SCI,

signifies 1 GFP⁺/ChAT⁺ motoneuron, quantified on 1 of 5 transverse sections. The pie charts in green (shRNA-CAPN1) and orange (shRNA-scramble) depict the proportion of motoneurons in each lumbar segment. (D) Top view of the 3D reconstructed whole lumbar spinal cord (ARIVIS visio4D software) after clearing, and ChAT immunolabeling shows the distribution of putative motoneurons either transduced (ChAT⁺/GFP⁺, yellow) or nontransduced (ChAT⁺/GFP⁻, red). (E and F) For quantification of transduced motoneurons (colocalization of immunolabelings), a horizontal 660- μ m slice containing rostro-caudal motoneuron columns was defined. (E) Schematic representation of the slice; (F) the resulting slice. (G) 3D rendering of the object maps representing the cells imported into the 3D ROI manager used for quantification of double-labeled motoneurons (GFP⁺/ChAT⁺, yellow).

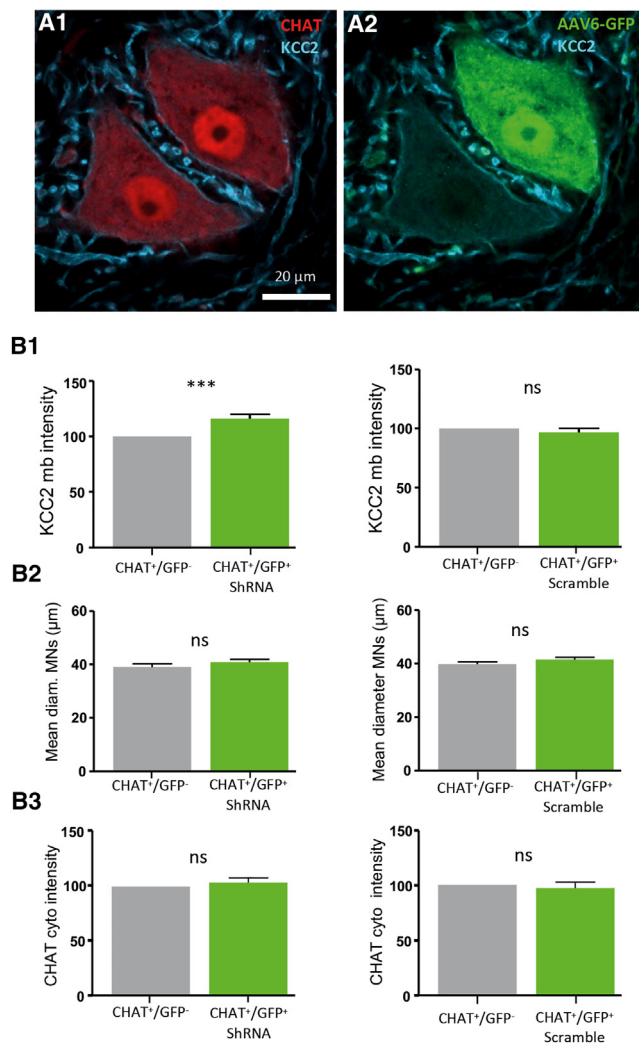


Figure 6. Increase in KCC2 membrane expression in shRNA-CAPN1-transduced lumbar motoneurons in rats with SCI

(A1 and A2) Example single optical sections showing immunostaining of ChAT (red) and KCC2 (blue) in a representative pair of motoneurons. (A1) One transduced (A2, GFP⁺, green) and the other nontransduced (A2, GFP⁻) by AAV6-GFP, 7 weeks after i.t. administration. Scale bar, 20 μm. (B1–B3) Comparisons of relative intensities of KCC2 immunostaining (B1), mean diameter of the soma (B2), and ChAT immunostaining (B3) between pairs of motoneurons nontransduced (gray) or transduced (green) by AAV6-GFP-shRNA-CAPN1 (B1, B2, and B3, left plots, n = 42 pairs) or by AAV6-GFP-shRNA-scramble (B1, B2, and B3, right plots, n = 67 pairs). Data are normalized to values quantified in nontransduced motoneurons (CHAT⁺/GFP⁻) and expressed as mean ± SEM. ***p < 0.001 (paired t test).

characterized by the progressive development of exaggerated spinal reflexes and increased muscle tone and spasms.^{46,51}

Silencing calpain1 in motoneurons restores the expression of KCC2 and alleviates spasticity

Our findings indicate that targeting calpain1 resulted in a widespread reduction in muscle spasms, with notable effects in the GS muscle,

whereas the TA muscle showed only a trend toward improvement. Although the transfection rates between TA and GS motoneurons were similar, we cannot dismiss the possibility of differences in calpain1 expression due to variations in the transcription/transduction processes within the flexor and extensor motor pools. This area warrants further exploration. In addition, it is important to consider that extensor and flexor motor pools may respond differently to SCI.⁵² This is particularly relevant because extensor motoneurons have a greater tendency to produce persistent inward currents and plateau potentials compared to flexor motoneurons.^{53,54}

Significant research efforts have been directed toward developing therapeutic strategies to inhibit calpains. Among various pharmacological inhibitors, MDL-28170, a cell membrane-penetrating aldehyde compound, has shown promise.⁵⁵ We previously demonstrated that MDL-28170 prevents the cleavage of both Nav1.6 and KCC2, thereby restoring motoneuron excitatory/inhibitory balance and reducing spasticity.^{12,13} Although we provide the proof of concept that the inhibition of calpains represents a rational curative treatment for spasticity after SCI, it is not applicable in medicine. The major issue is the lack of specificity insofar as inhibitors target calpain isoforms in an undifferentiated way, including calpain1 and calpain2, which are highly expressed in the nervous system. Furthermore, regarding the pleiotropic functions of calpains, their systemic inhibition is not advisable.⁵⁶

The next generation of treatments for spasticity may take advantage of genetic tools that allow the manipulation of a specific target, in specific cells, in a local circuit. We chose a viral transduction strategy to provide a proof of concept that the inhibition of calpain1¹³ may rebalance the excitatory/inhibitory equilibrium of motoneurons after SCI. In the present study, we report a significant 16% upregulation in KCC2 levels at the membrane of motoneurons transduced with AAV6-ShRNA-Calp1 (Figure 6). This increase identifies the activation of calpain1 as a key factor in the disinhibition of motoneurons after SCI. It is important to note that calpain-mediated cleavage of KCC2 has also been linked to disinhibition in other pathophysiological conditions.^{57–59} Our findings align with several preclinical studies that have successfully enhanced KCC2 expression in sublesional spinal motoneurons to alleviate spasticity. For instance, the i.t. injection of brain-derived neurotrophic factor or the activation of 5-HT_{2A} receptors has been shown to upregulate KCC2 levels by 11.8%, and 12%, respectively, contributing to reduce SCI-induced spasticity.^{16,17} Similarly, enhancing the Cl⁻ extrusion capacity of lumbar motoneurons with prochlorperazine led to an 11.4% increase in KCC2 levels.⁶⁰ Furthermore, exercise training associated with motor function recovery after SCI has been linked to a 12.2% increase in KCC2 levels below the injury site.⁸ Finally, the pharmacological inhibition of calpains has restored the levels of KCC2 in the ventral horn of SCT rats, effectively curtailing spasticity.¹³ Given that these previous studies have reinstated KCC2 expression to levels comparable to those in intact animals, our gene therapy approach, with its 16% increase in KCC2, likely reflects a similar restorative effect, offering a promising avenue for future treatment strategies.

From a clinical perspective, the delivery of AAVs is a promising route of administration in humans given the considerable progress being made in gene therapy research. Replication-defective viruses (rAAV) are capable of having long-term latency in mammalian cells and are therefore considered safe for use in virus-mediated human gene therapy.⁶¹ From a translational point of view, the i.t. delivery method appears feasible. However, the i.m. injection of AAVs, already used in animal models of neuromuscular diseases, seems more suitable for specifically targeting spastic muscles. This approach involves the retrograde transport of the vector to the motoneuron cell body connected to the injected muscles. However, our first trials are unsatisfactory. However, the engineering and profiling of viral vectors for gene delivery have undergone remarkable advances. In line with this, an interesting potential tool for future studies is the recombinant rAAV2-retro, whose single i.m. injection in neonatal mice enabled the extensive transduction of lower motoneurons in the spinal cord.^{61,62} If the rAAV2-retro also proves to be efficient in adult animals, then its peculiar features of retrograde axonal transduction would permit the selective performance of injections in spastic muscles of the limbs and the transduction of limited motoneuron pools.

MATERIALS AND METHODS

Animals

Experiments were performed on 42 adult Wistar Han female rats (220–280 g, Charles River). All of the procedures were approved by the Ethics Committee in Neurosciences at the Institut de Neurosciences de la Timone, INT-Marseille (APAFIS#27010).

EMG electrodes implantation

To assess muscle activity in the hindlimbs, and in particular cocontractions, surface electrodes were implanted on the GS and TA antagonist muscles (ankle extensor and flexor, respectively). The rats were initially anesthetized with 5% isoflurane and maintained under anesthesia with 1%–2% isoflurane via a mask. To avoid drying of the cornea, an ophthalmic cream (Dulcis, 25,000 IU/100 g, Allergan France Laboratories) was applied on the eyes. A subcutaneous (s.c.) injection of antibiotics (amoxicillin, 100 mg/kg; Clamoxyl, Merial) was also administered. After shaving the back and the hind leg, the skin was cleaned with Betadine (Betadine yellow 10% and Betadine red 4%; Mylan). The rats were placed on a heating plate to maintain their temperature at ~38°C. After local administration of xylocaine (1%; AstraZeneca), 3 skin incisions were made while the animal was in a ventral position: 2 longitudinal incisions along the lumbar and thoracic areas (under the clavicles) and 1 over the GS muscle on the right hind leg. The most rostral incision was for inserting a connector plug connected to an amplifier for EMG recordings. This plug was passed under the skin, with only the top protruding through the incision, minimizing the need for skin sutures. A pad placed under the skin connected 5 wired electrodes (including a ground electrode; s.c. electrodes E363/76/Spc, Bilaney Consultants GmbH). The wires were tunneled s.c. to the third incision on the paw, carefully avoiding the path for subsequent i.t. injections. Two electrodes were positioned on the GS muscle and 2 on the TA muscle, secured by ligation and adhesive (Surgibond). The incisions were then sutured with nonabsorbable thread (5-0 Ethicon, Mersuture,

polyester). After surgery, the rats received s.c. injections of warm saline (0.9%, 37°C, 2.5 mL) for hydration and recovery.

Lesion surgery

Rats were anesthetized with intraperitoneal (i.p.) injections of a mixture of ketamine (50 mg/kg Imalgene, Merial) and domitor (0.25 mg/kg, Medetomidine, Janssen). The spinal cord was then transected at the thoracic T8–T9 level after laminectomy. After SCI, animals received 5 mL of NaCl s.c. and were kept warm with food available until they awoke. Buprenorphine (0.05 mg/kg, Vetergesic, Sogeva) was administered twice over 24 h for pain management. Twice per day, their bladder was manually emptied until recovery of urinary function, their temperature and hydration were checked, and any clinical sign of pain was observed. One week postinjury, the rats were housed in pairs under a 12-h light/dark cycle with free access to food and water.

Retrograde labeling of motoneurons

To identify the GS and TA motoneuron pools, we performed retrograde labeling in adult rats ($n = 3$). The rats were anesthetized by i.p. administration of a mixture of ketamine (60 mg/kg, Imalgene, Merial) and xylazine (10 mg/kg, Rompun, Bayer). They received bilateral injections of fast blue (0.5% in NaCl 0.9%, Sigma, 10 μ L) in the TA muscle and cholera toxin β subunit-fluorescein isothiocyanate (1/100 in H₂O; Sigma Aldrich, 20 μ L) in the medial GS muscle. Seven days after injection, animals were perfused and the lumbar spinal cord was serially cut in transverse sections.

AAV injection modes

We used recombinant AAV6-GFP-shRNA-CAPN1 (5'GTGG AACCGCATCCGAAATTA 3') and AAV6-GFP-shRNA-scramble (VectorBuilder) at titrations of 1.05×10^{13} genome copies (GC)/ml and 1.5×10^{13} GC/ml, respectively. Serotype 6 was chosen for its brain and skeletal muscle tropism⁶³ and retrograde transport efficiency in rats.³⁸ To optimize lumbar motoneuron transduction, 4 AAV6 injection protocols were tested on 18 control or SCT rats (Figure 1A): i.m. ($n = 5$), intrasciatic ($n = 3$), i.s. ($n = 7$), and i.t. ($n = 3$), with durations ranging from 3 to 7 weeks. Successful protocols in control rats were replicated in SCT rats. Animals were anesthetized with i.p. injections of a mixture of ketamine (50 mg/kg, Imalgene, Merial) and domitor (0.25 mg/kg, Medetomidine, Janssen). AAV neuronal transduction was assessed by cytoplasmic expression of GFP.

i.m. injection

AAV6-GFP-shRNA-CAPN1 solution was injected with a Hamilton syringe (26G, style 2, Dutscher) into the right GS muscle, at 6 sites (5 μ L each) to target the motor endplates whose location was defined previously⁶⁴ (Figure 2B).

Intrasciatic injection

An incision was made along the hindlimb, immediately caudal and parallel to the femur, and the sciatic nerve was exposed. A single injection of AAV6-shRNA (5 μ L) was performed using a 10- μ L Hamilton syringe with beveled needle (26G, style 2, Dutscher).

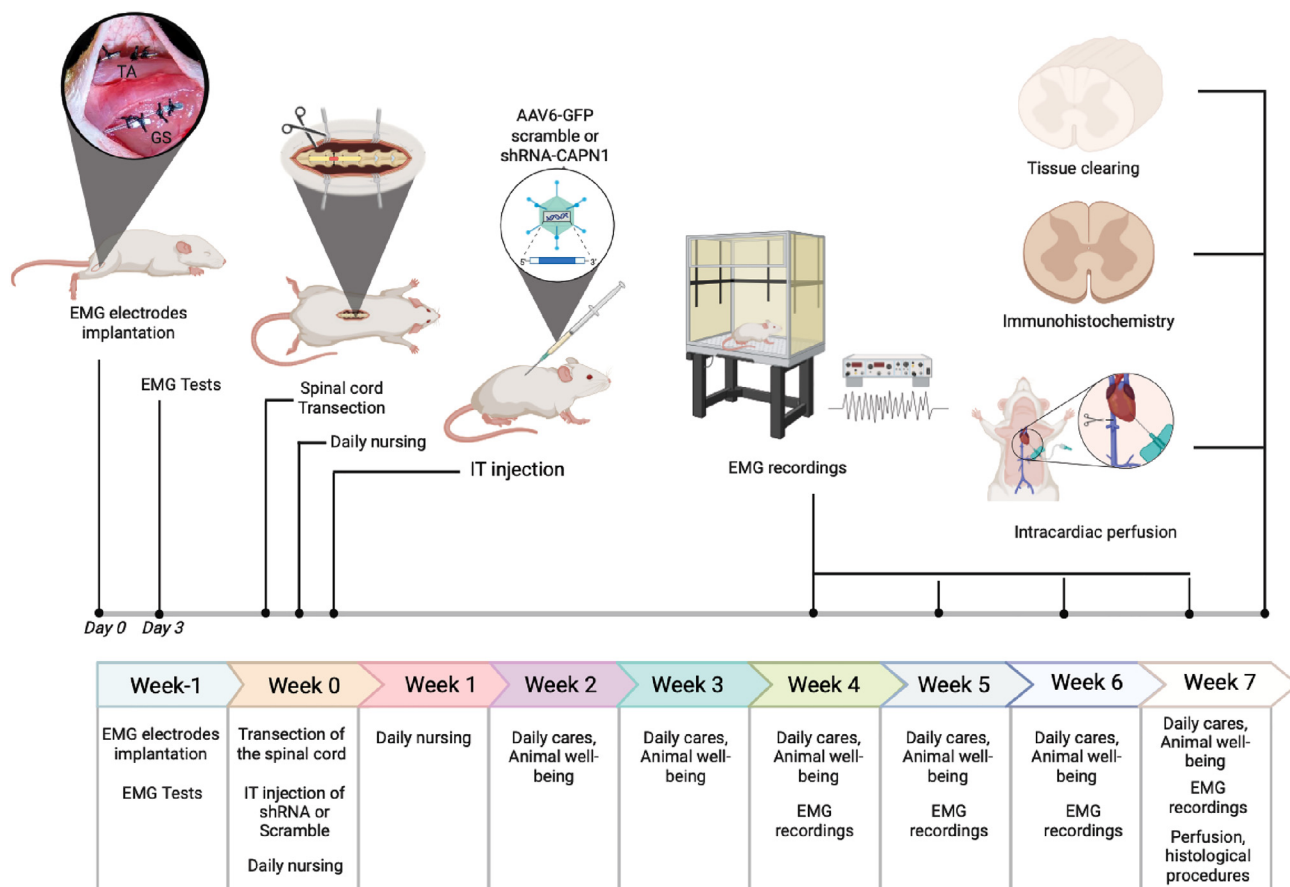


Figure 7. Time line and overview of the experimental procedures

The experimental procedures began with the implantation of EMG electrodes onto the GS and TA muscles 1 week before spinal cord transection (week –1), with EMG functionality tested in these intact animals. The following week (week 0), spinal cord transection at T8–T9 was performed, followed by a laminectomy at L2–L3 to facilitate i.t. injection of AAV6-GFP with either a scrambled sequence or shRNA-CAPN1. Subsequent care for the animals, including twice-daily nursing, continued until the end of week 3 postinjury. From week 4 to week 7 postinjury, the animals had daily access to an enriched environment to encourage free movement, with weekly EMG recordings to track muscular activity. The study was concluded in week 7, with the animals undergoing histological processing.

***i.s.* injection**

Following a laminectomy between T13 and L1 vertebrae, a single *i.s.* injection (1.2 μ L) of AAV6-GFP-shRNA (CAPN1 or scramble), was delivered using a 34G NanoFil *i.t.* cannula (Phymep) at a 20° angle (Figure 1C, upper diagram).

***i.t.* injection**

A laminectomy at L2 and L3 was followed by a *dura mater* incision. An *i.t.* catheter (32G, 18 cm, Phymep) was inserted rostrally to reach the L2 segment (Figure 1D, upper diagram). Four 5- μ L injections of AAV vector were administered, spaced 2 mm apart while retracting the catheter, to target the retrogradely identified GS and TA motoneuron regions.

Setting up the experimental procedure

The experimental protocol spanned 9 weeks and was divided into 2 series (Figure 7). One week before spinal transection (week –1), EMG

electrodes were implanted on the GS and TA muscles (Figure 7). Control EMG recordings were then performed on these neurologically intact animals. In the same surgical session (week 0), spinal transection at T8–T9 and laminectomy at L2–L3 for *i.t.* injections were performed (Figure 7). The rats were then randomized into 2 groups to receive *i.t.* injections of either AAV6-GFP-shRNA-CAPN1 or AAV6-GFP-shRNA-scramble. Postoperative care was provided twice daily until bladder function recovery. From weeks 2 to 3 postinjury, daily care continued, and for enrichment, rats were placed for 1 h/day in a group setting with *ad libitum* access to food and water (Figure 7). EMG recordings started at week 4 postinjury and continued weekly for 4 weeks (weeks 4–7; Figure 7). At the end of week 7 postinjury, animals were perfused for immunohistological processing (Figure 7).

Tissue clearing

The iDISCO method was used to carry out the tissue clearing. The process involved sequential dehydration in methanol solutions of

increasing concentrations (20%, 40%, 60%, 80%, and 100%, 1 h each at room temperature), followed by overnight incubation (OVN, gentle agitation), in 66% dichloromethane/33% methanol solution at room temperature. Samples were washed twice in 100% methanol and cooled at 4°C, before bleaching with 5% H₂O₂ in methanol, OVN, at 4°C. Tissues were rehydrated with a methanol/H₂O solution (80%, 60%, 40%, 20%, PBS 1×), 1 h each at room temperature. Samples were permeabilized in a solution of PBS/0.2% Triton X-100/20% DMSO/0.3 M glycine at 37°C (2 days), then blocked in a solution of PBS 1×/0.2% Triton X-100/10% DMSO/6% donkey serum at 37°C (3 days). Tissues were incubated (4 days) in primary antibody dilution in PBS/0.2% Tween 20 with 10 µg/mL heparin (PTWH) buffer completed with 5% DMSO and 3% donkey serum, then washed (1 day) with PTWH buffer. Secondary antibodies were diluted in the same buffer as primary antibodies without DMSO and incubated (4 days). After washing (1 day), samples were dehydrated as previously described. As a last step of the clearing technique, spinal cords were placed in a solution of 66% dichloromethane/33% methanol with shaking (3 h), then washed twice in 100% dichloromethane solution (total duration 30 min) to end in a dibenzyl ether solution.

Perfusion and sectioning

Animals were anesthetized with i.p. injections of a mixture of ketamine (50 mg/kg, Imalgene, Merial) and domitor (0.25 mg/kg, Medetomidine, Janssen) and perfused intracardially with 100 mL of PBS (0.1 M, pH 7.4), followed by 400 mL of 4% paraformaldehyde (in PBS 0.1 M, pH 7.3). Postfixation (2 h), lumbar spinal cords were rinsed in PBS, cryoprotected for 24 h in 30% sucrose, and frozen at -80°C. The lumbar segments were sectioned transversely at a 30-µm thickness using a cryostat (Microm) and collected serially (rostral-caudally) in 48-well plates filled with cryoprotective solution and stored at -20°C.

Immunohistochemical stainings

For each immunostaining series, 1 of 5 serial sections were mounted on microscope slides. To amplify intracytoplasmic GFP expression, an immunostaining amplification step was included in all of the procedures. The triple detection of KCC2, GFP, and ChAT was performed using a mixture of rabbit anti-KCC2 antibody (1:200, AB07432, Millipore), mouse anti-GFP (1:200, immunoglobulin G2a A111 20, Invitrogen) and goat anti-ChAT (AB 144P, Millipore). The double detection of calpain1 and GFP was performed using a mixture of rabbit calpain1 antibody (1:200, 2556S, Ozyme) and goat GFP antibody (1:1,000, AB5449, Abcam). This labeling was preceded by the incubation of the slices in a methanol solution for 3 h before immunostaining treatment. The secondary antibodies were Alexa 546-donkey anti-rabbit or anti-mouse (1:400, Invitrogen), Alexa 488-donkey anti-mouse (1:400, Invitrogen), and Alexa 633-donkey anti-goat or anti-rabbit (1:400, Invitrogen), respectively. Negative controls involved omitting primary antibodies, resulting in no labeling. After the clearing procedure, GFP/ChAT immunolabeling of the whole-mount lumbar spinal cord was performed using a mixture of rabbit anti-GFP (1:400, A111 22, Invitrogen) and goat anti-ChAT (1:200, AB 144P, Millipore). The secondary antibodies

were Alexa 488-donkey anti-rabbit (1:800 Invitrogen) and Alexa 546-donkey anti-goat (1:400, Invitrogen).

Cell culture

We used Lipofectamine 3000 (Thermo Fisher), to transiently cotransfect HEK293 cells with 2 plasmids: one encoding rat CAPN1 (VB230228-1069hct, VectorBuilder) and the other either encoding shRNA targeting CAPN1 or a control plasmid encoding shRNA against luciferase. The cells were then collected 72 h posttransfection.

Western blot

For the total fraction, HEK293 cells were homogenized in ice-cold lysis buffer (1% Igepal CA-630, 0.1% SDS) supplemented with protease inhibitors (CompleteMini, Roche Diagnostic). Insolubilized material was pelleted by centrifugation at 10,000 rpm for 10 min at 4°C. The supernatant corresponds to the total fraction. Protein concentrations were determined using a detergent-compatible protein assay (Bio-Rad). Equal protein amounts (40 µg) from denatured samples were size fractionated by 4%–15% gradient SDS/PAGE stain-free gel (Bio-Rad), transferred to a nitrocellulose membrane, and probed with the calpain1 polyclonal rabbit antibody (1:500, 2556s, Ozyme) or the actin polyclonal rabbit antibody (1:1,000, A2066, Sigma) at 4°C overnight in Tris-buffered saline containing 5% fat-free milk powder. The blot was then incubated 1 h at 22°C with an ImmunoPure goat horseradish peroxidase-conjugated rabbit-specific antibody (1:40,000 in blocking solution; Thermo Scientific). The blots were blotted with an enhanced chemiluminescence detection (Merck-Millipore). Signal intensities were measured with the image analysis software image Lab (Bio-Rad).

EMG analysis and processing

Muscle activities were recorded from weeks 4 to 7 postinjury, when signs of spasticity begin to be firmly established, including excessive muscle tone, spasms, and hyperreflexia. In our study, EMG recordings were conducted while rats moved freely in an open field. This setup involved a rotating connector positioned above the animals, which served as a link between the implanted plug on each rat's back and the recording equipment. We used an alternating current (AC)-coupled amplifier (Model 1700, A.M. Systems) for signal amplification. EMG recordings were amplified ($\times 1,000$), high-pass filtered at 300 Hz, low-pass filtered at 5 kHz, and sampled at 13.5 kHz (Digitdata 1440A, Molecular Devices). Our protocol involved weekly recordings of both spontaneous muscle activities and responses elicited by tail pinching. After a 20-min acclimation period in the open field, each recording session lasted 30 min per animal. The raw AC-mode signals were rectified and integrated using a custom Python script for data analysis. Spontaneous muscle contractions were identified when the signal's envelope surpassed a set threshold, with the contraction ending as the signal dropped back below this threshold. The threshold was tailored for each signal, usually set at 1.5 times the background noise level. To be classified as a valid muscle spasm, an event had to be above threshold for at least 500 ms. The program then aggregated the average duration, amplitude, and number of these events for each muscle, analyzing them in 15-min intervals. The script

calculated the instances in which bursts in the 2 EMG signals from antagonist muscles (GS vs. TA) overlapped, indicating cocontractions. It quantified the extent of overlapping as a percentage of the total number of muscle spasms. For responses triggered by tail stimulation, EMG data were quantified by summing spike counts in peristimulus time histograms, calculated over a 15-s period following stimulation, using a voltage peak detector.

Quantification of immunolabelings in confocal microscopy

Acquisitions were made at 40 \times oil objective (scanning confocal microscope ZEISS LSM 700). We selected fields with pairs of motoneurons including 1 transduced (ChAT⁺/GFP⁺) and 1 nontransduced (ChAT⁺/GFP⁻) motoneuron. Only pairs of motoneurons with clear visible nucleus and nucleolus were taken into consideration. Stacks of confocal images were acquired by sequential scanning for the 3 channels (488, 543, 633 nm excitation wavelengths). For each scan series, the intensity of each laser was adjusted under the threshold of saturation (red pixel in range indicator mode). For each motoneuron, we determined the surface of the membrane, delimited by overlaying the internal and external borders of the KCC2-immunolabeled membrane.¹⁶ Within this membrane surface area, we measured the mean pixel intensity of the immunolabeling fluorescence of KCC2. We also measured the mean fluorescence intensity in the 3 channels within the cytoplasm of the motoneurons, as well as their mean diameter ((large + small diameter)/2). For relative comparison of the fluorescence intensities in the different experimental groups, measurements were normalized, as previously performed.^{14,16,17}

Image analysis and processing after tissue clearing

After the clearing procedure, mosaic acquisition of the lumbar spinal cords was made at 12 \times magnification, zoom 0.66 (Lightsheet microscope, Miltenyi Biotec). ARIVIS visio4D software was used to reconstruct the sample three dimensionally (3D). Fiji⁶⁵ was used for image visualization. To quantify 3D colocalization from cleared tissue images, the following plugins were used in Fiji. Images were background subtracted through the rolling ball algorithm. To correct for minimal horizontal drift between acquisitions of different channels, the StakReg plugin was used.⁶⁶ To sharpen the edges of the particles to analyze, we used the Difference-of-Gaussians filter in CLIJ2.⁶⁷ Afterward, object maps were filtered based on their size using the MorphoLibJ filter Grayscale Attribute Filtering 3D plugin.⁶⁸ To obtain 3D object maps representing the cells, we used the 3D object counter⁶⁹ in its CLIJ2 version.⁶⁷ Then, objects maps were imported into the 3D ROI (region of interest) manager from the 3D suite⁷⁰ also used for quantification. The 3D mask obtained from the ChAT immunolabeling (motoneurons, 543 nm, red) channel was imposed over the GFP (transfected motoneurons, 488 nm, green) channel to obtain the immunoreactivity values. To establish a cutoff value for colocalization, the GFP image was Gaussian blurred in an iterative manner until the edges of the objects were undistinguishable. The 3D mask of all ChAT particles was then applied over this image, and the obtained median value plus 2xSD was used as the threshold value to define colocalization. Multi-ROI selection in the 3D ROI manager was performed through scripts, and 3 sets of images were

created (whole ChAT⁺ population, ChAT⁺ colocalizing with GFP⁺, and ChAT⁺ noncolocalizing with GFP⁺). Rendering was done through Fiji and/or UCSF Chimera Software.⁷¹

Statistical analysis

No statistical method was used to predetermine the sample size. Group measurements were expressed as means \pm SEMs. When 2 groups were compared, we used the unpaired Mann-Whitney test or the unpaired t test. We also used 2-way ANOVA tests for multiple comparisons. For all of the statistical analyses, the data met the assumptions of the test, and the variance between the statistically compared groups was similar. The level of significance was set at $p < 0.05$. Statistical analyses were performed using GraphPad Prism 7 software and are indicated in the figure legends.

DATA AND CODE AVAILABILITY

All of the original data are available from the authors without any restriction.

ACKNOWLEDGMENTS

Surgery, postoperative care, and nursing were performed by NSrepair, Inc., INT, Marseille, France. We are grateful to Geneviève Rougon for revising the manuscript. This work was supported by AMU, CNRS, ANR CalpaSci grants to F.B. and M.B. and an ANR SpasT-SCI-T grant to F.B.

AUTHOR CONTRIBUTIONS

F.B. and H.B. conceptualized the study. C.B., M.K., and H.B. performed the immunostaining. C.B. performed the tissue clearing. V.T. performed the culture experiments. H.B. performed the *in vivo* experiments. M.K., C.B., J.V., F.B., J.J.R.F., and H.B. performed the analysis. F.B., C.B., J.V., and H.B. created the figures. J.V., N.D., F.B., and H.B. wrote the manuscript. N.D., C.B., F.B., M.B., and H.B. contributed to the final version of the manuscript.

DECLARATION OF INTERESTS

The authors declare no competing interests.

REFERENCES

- Adams, M.M., and Hicks, A.L. (2005). Spasticity after spinal cord injury. *Spinal Cord* 43, 577–586.
- D'Amico, J.M., Condliffe, E.G., Martins, K.J.B., Bennett, D.J., and Gorassini, M.A. (2014). Recovery of neuronal and network excitability after spinal cord injury and implications for spasticity. *Front. Integr. Neurosci.* 8, 36. <https://doi.org/10.3389/fnint.2014.00036>.
- Bensmail, D., Wissel, J., Laffont, I., Simon, O., Scheschonka, A., Flatau-Baqué, B., Dressler, D., and Simpson, D.M. (2021). Efficacy of incobotulinumtoxinA for the treatment of adult lower-limb post-stroke spasticity, including pes equinovarus. *Ann. Phys. Rehabil. Med.* 64, 101376. <https://doi.org/10.1016/j.rehab.2020.03.005>.
- Hultborn, H. (2003). Changes in neuronal properties and spinal reflexes during development of spasticity following spinal cord lesions and stroke: studies in animal models and patients. *J. Rehabil. Med.* 35, 46–55.
- Gorassini, M.A., Knash, M.E., Harvey, P.J., Bennett, D.J., and Yang, J.F. (2004). Role of motoneurons in the generation of muscle spasms after spinal cord injury. *Brain* 127, 2247–2258. <https://doi.org/10.1093/brain/awh243>.

6. Biering-Sorensen, F., Nielsen, J.B., and Klinge, K. (2006). Spasticity-assessment: a review. *Spinal Cord* 44, 708–722.
7. Beverungen, H., Klaszky, S.C., Klaszky, M., and Côté, M.P. (2020). Rehabilitation Decreases Spasticity by Restoring Chloride Homeostasis through the Brain-Derived Neurotrophic Factor-KCC2 Pathway after Spinal Cord Injury. *J. Neurotrauma* 37, 846–859. <https://doi.org/10.1089/neu.2019.6526>.
8. Côté, M.P., Gandhi, S., Zambrotta, M., and Houlé, J.D. (2014). Exercise modulates chloride homeostasis after spinal cord injury. *J. Neurosci.* 34, 8976–8987.
9. Li, Y., and Bennett, D.J. (2003). Persistent sodium and calcium currents cause plateau potentials in motoneurons of chronic spinal rats. *J. Neurophysiol.* 90, 857–869. <https://doi.org/10.1152/jn.00236.2003>.
10. Harvey, P.J., Li, Y., Li, X., and Bennett, D.J. (2006). Persistent sodium currents and repetitive firing in motoneurons of the sacrocaudal spinal cord of adult rats. *J. Neurophysiol.* 96, 1141–1157. <https://doi.org/10.1152/jn.00335.2005>.
11. ElBasiouny, S.M., Schuster, J.E., and Heckman, C.J. (2010). Persistent inward currents in spinal motoneurons: important for normal function but potentially harmful after spinal cord injury and in amyotrophic lateral sclerosis. *Clin. Neurophysiol.* 121, 1669–1679. <https://doi.org/10.1016/j.clinph.2009.12.041>.
12. Brocard, C., Plantier, V., Boulenguez, P., Liabeuf, S., Bouhadfane, M., Viallat-Lieutaud, A., Vinay, L., and Brocard, F. (2016). Cleavage of Na(+) channels by calpain increases persistent Na(+) current and promotes spasticity after spinal cord injury. *Nat. Med.* 22, 404–411.
13. Plantier, V., Sanchez-Brualla, I., Dingu, N., Brocard, C., Liabeuf, S., Gackière, F., and Brocard, F. (2019). Calpain fosters the hyperexcitability of motoneurons after spinal cord injury and leads to spasticity. *Elife* 8, e51404. <https://doi.org/10.7554/eLife.51404>.
14. Sadlaoud, K., Khalki, L., Brocard, F., Vinay, L., Boulenguez, P., and Bras, H. (2020). Alteration of glycinergic receptor expression in lumbar spinal motoneurons is involved in the mechanisms underlying spasticity after spinal cord injury. *J. Chem. Neuroanat.* 106, 101787. <https://doi.org/10.1016/j.jchemneu.2020.101787>.
15. Bras, H., and Liabeuf, S. (2021). Differential effects of spinal cord transection on glycinergic and GABAergic synaptic signaling in sub-lesional lumbar motoneurons. *J. Chem. Neuroanat.* 113, 101847. <https://doi.org/10.1016/j.jchemneu.2020.101847>.
16. Boulenguez, P., Liabeuf, S., Bos, R., Bras, H., Jean-Xavier, C., Brocard, C., Stil, A., Darbon, P., Cattaert, D., Delpire, E., et al. (2010). Down-regulation of the potassium-chloride cotransporter KCC2 contributes to spasticity after spinal cord injury. *Nat. Med.* 16, 302–307.
17. Bos, R., Sadlaoud, K., Boulenguez, P., Buttigieg, D., Liabeuf, S., Brocard, C., Haase, G., Bras, H., and Vinay, L. (2013). Activation of 5-HT2A receptors upregulates the function of the neuronal K-Cl cotransporter KCC2. *Proc. Natl. Acad. Sci. USA* 110, 348–353. <https://doi.org/10.1073/pnas.1213680110>.
18. Módol, L., Mancuso, R., Alé, A., Francos-Quijorna, I., and Navarro, X. (2014). Differential effects on KCC2 expression and spasticity of ALS and traumatic injuries to motoneurons. *Front. Cell. Neurosci.* 8, 7. <https://doi.org/10.3389/fncel.2014.00007>.
19. Klomjai, W., Roche, N., Lamy, J.C., Bede, P., Giron, A., Bussel, B., Bensmail, D., Katz, R., and Lackmy-Vallée, A. (2019). Furosemide Unmasks Inhibitory Dysfunction after Spinal Cord Injury in Humans: Implications for Spasticity. *J. Neurotrauma* 36, 1469–1477. <https://doi.org/10.1089/neu.2017.5560>.
20. Nickolls, P., Collins, D.F., Gorman, R.B., Burke, D., and Gandevia, S.C. (2004). Forces consistent with plateau-like behaviour of spinal neurons evoked in patients with spinal cord injuries. *Brain*. 127, 660–670.
21. Hornby, T.G., Rymer, W.Z., Benz, E.N., and Schmit, B.D. (2003). Windup of flexion reflexes in chronic human spinal cord injury: a marker for neuronal plateau potentials? *J. Neurophysiol.* 89, 416–426. <https://doi.org/10.1152/jn.00979.2001>.
22. Collins, D.F., Burke, D., and Gandevia, S.C. (2001). Large involuntary forces consistent with plateau-like behavior of human motoneurons. *J. Neurosci.* 21, 4059–4065.
23. Bennett, D.J., Li, Y., Harvey, P.J., and Gorassini, M. (2001). Evidence for plateau potentials in tail motoneurons of awake chronic spinal rats with spasticity. *J. Neurophysiol.* 86, 1972–1982. <https://doi.org/10.1152/jn.2001.86.4.1972>.
24. Murray, K.C., Nakae, A., Stephens, M.J., Rank, M., D'Amico, J., Harvey, P.J., Li, X., Harris, R.L.W., Ballou, E.W., Anelli, R., et al. (2010). Recovery of motoneuron and locomotor function after spinal cord injury depends on constitutive activity in 5-HT2C receptors. *Nat. Med.* 16, 694–700. <https://doi.org/10.1038/nm.2160>.
25. Goll, D.E., Thompson, V.F., Li, H., Wei, W., and Cong, J. (2003). The calpain system. *Physiol. Rev.* 83, 731–801. <https://doi.org/10.1152/physrev.00029.2002>.
26. Banik, N.L., Matzelle, D.C., Gantt-Wilford, G., Osborne, A., and Hogan, E.L. (1997). Increased calpain content and progressive degradation of neurofilament protein in spinal cord injury. *Brain Res.* 752, 301–306.
27. Springer, J.E., Azbill, R.D., Kennedy, S.E., George, J., and Geddes, J.W. (1997). Rapid calpain I activation and cytoskeletal protein degradation following traumatic spinal cord injury: attenuation with riluzole pretreatment. *J. Neurochem.* 69, 1592–1600.
28. Schumacher, P.A., Eubanks, J.H., and Fehlings, M.G. (1999). Increased calpain I-mediated proteolysis, and preferential loss of dephosphorylated NF200, following traumatic spinal cord injury. *Neuroscience* 91, 733–744.
29. Li, Z., Hogan, E.L., and Banik, N.L. (1996). Role of calpain in spinal cord injury: increased calpain immunoreactivity in rat spinal cord after impact trauma. *Neurochem. Res.* 21, 441–448.
30. Yu, C.G., Li, Y., Raza, K., Yu, X.X., Ghoshal, S., and Geddes, J.W. (2013). Calpain 1 knockdown improves tissue sparing and functional outcomes after spinal cord injury in rats. *J. Neurotrauma* 30, 427–433. <https://doi.org/10.1089/neu.2012.2561>.
31. Shields, D.C., Schaecher, K.E., Hogan, E.L., and Banik, N.L. (2000). Calpain activity and expression increased in activated glial and inflammatory cells in penumbra of spinal cord injury lesion. *J. Neurosci. Res.* 61, 146–150. [https://doi.org/10.1002/1097-4547\(20000715\)61:2<146](https://doi.org/10.1002/1097-4547(20000715)61:2<146).
32. Stepankova, K., Jendelova, P., and Machova Urdzikova, L. (2021). Planet of the AAVs: The Spinal Cord Injury Episode. *Biomedicines* 9, 613. <https://doi.org/10.3390/biomedicines9060613>.
33. Mendonça, R.H., and Zanoteli, E. (2022). Gene therapy in neuromuscular disorders. *Arq. Neuropsiquiatr.* 80, 249–256. <https://doi.org/10.1590/0004-282x-arp-2022-s135>.
34. Kaspar, B.K., Lladó, J., Sherkat, N., Rothstein, J.D., and Gage, F.H. (2003). Retrograde viral delivery of IGF-1 prolongs survival in a mouse ALS model. *Science (New York, N.Y.)* 301, 839–842. <https://doi.org/10.1126/science.1086137>.
35. Towne, C., Setola, V., Schneider, B.L., and Aebischer, P. (2011). Neuroprotection by gene therapy targeting mutant SOD1 in individual pools of motor neurons does not translate into therapeutic benefit in fALS mice. *Mol. Ther.* 19, 274–283. <https://doi.org/10.1038/mt.2010.260>.
36. Ayers, J.I., Fromholt, S., Sinyavskaya, O., Siemienski, Z., Rosario, A.M., Li, A., Crosby, K.W., Cruz, P.E., DiNunno, N.M., Janus, C., et al. (2015). Widespread and efficient transduction of spinal cord and brain following neonatal AAV injection and potential disease modifying effect in ALS mice. *Mol. Ther.* 23, 53–62. <https://doi.org/10.1038/mt.2014.180>.
37. Benkhelifa-Ziyyat, S., Besse, A., Roda, M., Duque, S., Astord, S., Carcenac, R., Marais, T., and Barkats, M. (2013). Intramuscular scAAV9-SMN injection mediates widespread gene delivery to the spinal cord and decreases disease severity in SMA mice. *Mol. Ther.* 21, 282–290. <https://doi.org/10.1038/mt.2012.261>.
38. Hollis Ii, E.R., Kadoya, K., Hirsch, M., Samulski, R.J., and Tuszyński, M.H. (2008). Efficient retrograde neuronal transduction utilizing self-complementary AAV1. *Mol. Ther.* 16, 296–301. <https://doi.org/10.1038/sj.mt.6300367>.
39. Duque, S., Joussemet, B., Riviere, C., Marais, T., Dubreil, L., Douar, A.M., Fyfe, J., Moullier, P., Colle, M.A., and Barkats, M. (2009). Intravenous administration of self-complementary AAV9 enables transgene delivery to adult motor neurons. *Mol. Ther.* 17, 1187–1196. <https://doi.org/10.1038/mt.2009.71>.
40. Wu, R., Wang, H., Xia, X., Zhou, H., Liu, C., Castro, M., and Xu, Z. (2009). Nerve injection of viral vectors efficiently transfers transgenes into motor neurons and delivers RNAi therapy against ALS. *Antioxid. Redox Signal.* 11, 1523–1534. <https://doi.org/10.1089/ars.2009.2618>.
41. Dayton, R.D., Wang, D.B., and Klein, R.L. (2012). The advent of AAV9 expands applications for brain and spinal cord gene delivery. *Expert Opin. Biol. Ther.* 12, 757–766. <https://doi.org/10.1517/14712598.2012.681463>.
42. Tanguy, Y., Biferi, M.G., Besse, A., Astord, S., Cohen-Tannoudji, M., Marais, T., and Barkats, M. (2015). Systemic AAVrh10 provides higher transgene expression than

- AAV9 in the brain and the spinal cord of neonatal mice. *Front. Mol. Neurosci.* 8, 36. <https://doi.org/10.3389/fnmol.2015.00036>.
43. Foust, K.D., Nurre, E., Montgomery, C.L., Hernandez, A., Chan, C.M., and Kaspar, B.K. (2009). Intravascular AAV9 preferentially targets neonatal neurons and adult astrocytes. *Nat. Biotechnol.* 27, 59–65. <https://doi.org/10.1038/nbt.1515>.
44. Snyder, B.R., Gray, S.J., Quach, E.T., Huang, J.W., Leung, C.H., Samulski, R.J., Boulis, N.M., and Federici, T. (2011). Comparison of adeno-associated viral vector serotypes for spinal cord and motor neuron gene delivery. *Hum. Gene Ther.* 22, 1129–1135. <https://doi.org/10.1089/hum.2011.008>.
45. Salegio, E.A., Samaranch, L., Kells, A.P., Mittermeyer, G., San Sebastian, W., Zhou, S., Beyer, J., Forsayeth, J., and Bankiewicz, K.S. (2013). Axonal transport of adeno-associated viral vectors is serotype-dependent. *Gene Ther.* 20, 348–352. <https://doi.org/10.1038/gt.2012.27>.
46. Hiersemenzel, L.P., Curt, A., and Dietz, V. (2000). From spinal shock to spasticity: neuronal adaptations to a spinal cord injury. *Neurology* 54, 1574–1582. <https://doi.org/10.1212/wnl.54.8.1574>.
47. Hsieh, T.H., Tsai, J.Y., Wu, Y.N., Hwang, I.S., Chen, T.I., and Chen, J.J.J. (2010). Time course quantification of spastic hypertonia following spinal hemisection in rats. *Neuroscience* 167, 185–198. <https://doi.org/10.1016/j.neuroscience.2010.01.064>.
48. Bose, P., Parmer, R., and Thompson, F.J. (2002). Velocity-dependent ankle torque in rats after contusion injury of the midthoracic spinal cord: time course. *J. Neurotrauma* 19, 1231–1249.
49. Bennett, D.J., Sanelli, L., Cooke, C.L., Harvey, P.J., and Gorassini, M.A. (2004). Spastic long-lasting reflexes in the awake rat after sacral spinal cord injury. *J. Neurophysiol.* 91, 2247–2258. <https://doi.org/10.1152/jn.00946.2003>.
50. Krenz, N.R., and Weaver, L.C. (1998). Sprouting of primary afferent fibers after spinal cord transection in the rat. *Neuroscience* 85, 443–458. [https://doi.org/10.1016/s0306-4522\(97\)00622-2](https://doi.org/10.1016/s0306-4522(97)00622-2).
51. Malmsten, J. (1983). Time course of segmental reflex changes after chronic spinal cord hemisection in the rat. *Acta Physiol. Scand.* 119, 435–443. <https://doi.org/10.1111/j.1748-1716.1983.tb07359.x>.
52. Khalki, L., Sadlaoud, K., Lerond, J., Coq, J.O., Brezun, J.M., Vinay, L., Coulon, P., and Bras, H. (2018). Changes in innervation of lumbar motoneurons and organization of premotor network following training of transected adult rats. *Exp. Neurol.* 299, 1–14. <https://doi.org/10.1016/j.expneurol.2017.09.002>.
53. Cotel, F., Antri, M., Barthe, J.Y., and Orsal, D. (2009). Identified ankle extensor and flexor motoneurons display different firing profiles in the neonatal rat. *J. Neurosci.* 29, 2748–2753. <https://doi.org/10.1523/jneurosci.3462-08.2009>.
54. Hounsgaard, J., Hultborn, H., Jespersen, B., and Kiehn, O. (1988). Bistability of alpha-motoneurons in the decerebrate cat and in the acute spinal cat after intravenous 5-hydroxytryptophan. *J. Physiol.* 405, 345–367. <https://doi.org/10.1113/jphysiol.1988.sp017336>.
55. Dókus, L.E., Yousef, M., and Bánóczy, Z. (2020). Modulators of calpain activity: inhibitors and activators as potential drugs. *Expert Opin. Drug Discov.* 15, 471–486. <https://doi.org/10.1080/17460441.2020.1722638>.
56. Ono, Y., Saïdo, T.C., and Sorimachi, H. (2016). Calpain research for drug discovery: challenges and potential. *Nat. Rev. Drug Discov.* 15, 854–876. <https://doi.org/10.1038/nrd.2016.212>.
57. Zhou, H.Y., Chen, S.R., Byun, H.S., Chen, H., Li, L., Han, H.D., Lopez-Berestein, G., Sood, A.K., and Pan, H.L. (2012). N-methyl-D-aspartate receptor- and calpain-mediated proteolytic cleavage of K⁺-Cl⁻ cotransporter-2 impairs spinal chloride homeostasis in neuropathic pain. *J. Biol. Chem.* 287, 33853–33864. <https://doi.org/10.1074/jbc.M112.395830>.
58. Puskarjov, M., Ahmad, F., Kaila, K., and Blaesse, P. (2012). Activity-dependent cleavage of the K-Cl cotransporter KCC2 mediated by calcium-activated protease calpain. *J. Neurosci.* 32, 11356–11364.
59. Wan, L., Ren, L., Chen, L., Wang, G., Liu, X., Wang, B.H., and Wang, Y. (2018). M-Calpain Activation Facilitates Seizure Induced KCC2 Down Regulation. *Front. Mol. Neurosci.* 11, 287. <https://doi.org/10.3389/fnmol.2018.00287>.
60. Liabeuf, S., Stuhl-Gourmand, L., Gackière, F., Mancuso, R., Sanchez Brualla, I., Marino, P., Brocard, F., and Vinay, L. (2017). Prochlorperazine Increases KCC2 Function and Reduces Spasticity after Spinal Cord Injury. *J. Neurotrauma* 34, 3397–3406. <https://doi.org/10.1089/neu.2017.5152>.
61. Chen, Z., Fan, G., Li, A., Yuan, J., and Xu, T. (2020). rAAV2-Retro Enables Extensive and High-Efficient Transduction of Lower Motor Neurons following Intramuscular Injection. *Mol. Ther. Methods Clin. Dev.* 17, 21–33. <https://doi.org/10.1016/j.omtm.2019.11.006>.
62. Drouillas, B., Brocard, C., Zanella, S., Bos, R., and Brocard, F. (2023). Persistent Nav1.1 and Nav1.6 currents drive spinal locomotor functions through nonlinear dynamics. *Cell Rep.* 42, 113085. <https://doi.org/10.1016/j.celrep.2023.113085>.
63. Blankinship, M.J., Gregorevic, P., Allen, J.M., Harper, S.Q., Harper, H., Halbert, C.L., Miller, A.D., and Chamberlain, J.S. (2004). Efficient transduction of skeletal muscle using vectors based on adeno-associated virus serotype 6. *Mol. Ther.* 10, 671–678. <https://doi.org/10.1016/j.ymthe.2004.07.016>.
64. Ma, J., Smith, B.P., Smith, T.L., Walker, F.O., Rosencrance, E.V., and Koman, L.A. (2002). Juvenile and adult rat neuromuscular junctions: density, distribution, and morphology. *Muscle Nerve* 26, 804–809. <https://doi.org/10.1002/mus.10272>.
65. Schindelin, J., Arganda-Carreras, I., Frise, E., Kaynig, V., Longair, M., Pietzsch, T., Preibisch, S., Rueden, C., Saalfeld, S., Schmid, B., et al. (2012). Fiji: an open-source platform for biological-image analysis. *Nat. Methods* 9, 676–682. <https://doi.org/10.1038/nmeth.2019>.
66. Thévenaz, P., Ruttimann, U.E., and Unser, M. (1998). A pyramid approach to sub-pixel registration based on intensity. *IEEE Trans. Image Process.* 7, 27–41. <https://doi.org/10.1109/83.650848>.
67. Haase, R., Royer, L.A., Steinbach, P., Schmidt, D., Dibrov, A., Schmidt, U., Weigert, M., Maghelli, N., Tomancak, P., Jug, F., and Myers, E.W. (2020). CLIJ: GPU-accelerated image processing for everyone. *Nat. Methods* 17, 5–6. <https://doi.org/10.1038/s41592-019-0650-1>.
68. Legland, D., Arganda-Carreras, I., and Andrey, P. (2016). MorphoLibJ: integrated library and plugins for mathematical morphology with ImageJ. *Bioinformatics (Oxford, England)* 32, 3532–3534. <https://doi.org/10.1093/bioinformatics/btw413>.
69. Bolte, S., and Cordelières, F.P. (2006). A guided tour into subcellular colocalization analysis in light microscopy. *J. Microsc.* 224, 213–232. <https://doi.org/10.1111/j.1365-2818.2006.01706.x>.
70. Ollion, J., Cochenne, J., Loll, F., Escudé, C., and Boudier, T. (2013). TANGO: a generic tool for high-throughput 3D image analysis for studying nuclear organization. *Bioinformatics (Oxford, England)* 29, 1840–1841. <https://doi.org/10.1093/bioinformatics/btt276>.
71. Pettersen, E.F., Goddard, T.D., Huang, C.C., Couch, G.S., Greenblatt, D.M., Meng, E.C., and Ferrin, T.E. (2004). UCSF Chimera—a visualization system for exploratory research and analysis. *J. Comput. Chem.* 25, 1605–1612. <https://doi.org/10.1002/jcc.20084>.